Pakistan Journal of Information and Technology, 1(3): 242-249, 2002
© Copyright by the Science Publications, 2002

Simulation of Vortex Flows in Axial Flow Fan Using Computational Fluid Dynamics

E. E. Elhadi and Wu Keqi
School of Energy and Power Engineering, Huazhong University of Science and Technology
Wuhan, 430074, China

Abstract: This work aims to study and analyze the behavior of flow in axial flow fan. Numerical simulations were carried out based on Navier-Stoke equations coupled with $k-\varepsilon$ Turbulence model with standard wall function. These simulations were applied to axial flow fan which consists of nine rotor blades and fifteen stator blades. These blades were designed by modified quasi-three dimensional design program code. In the present work, different flow phenomena which occur in axial flow fan were presented and interpreted at different regions with special concern to the rotor exit and stator regions. In order to study the behavior and mechanism of these phenomena, different flow parameters (velocity components, pressure, and turbulent intensity) were calculated at different regions and at different flow rate coefficients. It is found that high flow rate causes higher vortex flow than low flow rate, mainly due to existence of the adverse pressure and hence a reverse flow at high flow rate. This is clearly observed in the stator region which negatively affected by increasing the flow rate and the stator became inefficient. It has been also found that, high flow rate causes a vortex flow at stator pressure side while the lower flow rate causes a vortex flow at stator suction side. This study shows that decrease in flow rate causes wider range of wake and vortex at the rotor exit than that caused by the other cases of flow rate. Finally in order to validate the present simulation, the obtained results were compared with the available literature results and it was found that their physical behavior agree quite well.

Key Words: Axial Flow Fan, Secondary Flow, Wake, Vortex and CFD

Introduction

Turbo machinery flows modeling requires built in capabilities for the assessment of viscous and turbulent effects on secondary flow (end wall losses, flow turning, flow separation, etc). Highly efficient numerical simulation is required to study and analyze different flow phenomena which occur in turbomachinery passage. Due to advances in high speed computers, an accurate computation of three dimensional turbomachinery flow field is now feasible. (Chen naixing, 2001) used numerical method to analyze and discus the generation and the evolution of secondary flow and vortices in turbine blade passage. He stated that using CFD calculations many phenomena inside turbo machinery can be predicted and modified if it is serious. Su moming (1996) studied the complete three-dimensional flow field in axial flow impeller. He developed a computational procedure to predict three dimensional incompressible separated turbulent flows in impeller. Chen *et al.*, (1999) developed a computational method based on a pressure correction technique and coupled by $k-\varepsilon$ model to study three dimensional viscous flow in axial flow compressor. Motoo (1982) developed a periodic measuring system to measure a three dimensional flow field and turbulent characteristics behind axial impeller. Chang (2000) studied the performance characteristics of an industrial vane axial fan and three dimensional flow field at the rotor exit using experimental test.

The present numerical tool is used to gain insight into the complex three-dimensional (3D) flow developing in axial flow fan (consists of nine rotor blades and fifteen stator blades) of free vortex design, with special concern to the wake passage vortex at the rotor exit and stator region at different flow rate values. In fact, most if not all, of the flow characteristics of the turbo machinery flow field phenomena are dependent upon the required flow rate. There fore, this study aims to not only study the characteristics of different flow field phenomena in general sense, but also to isolate how these characteristics change with different flow rate values.

In the present simulation, the axial flow fan blades were designed by modified quasi-three-dimensional (q-3-D) code based on solving the meridional flow and selecting the blade element using NACA cascade data. Numerical simulation was carried out using Navier Stoke equations coupled by $k-\varepsilon$ turbulent model with standard wall functions. Boundary conditions were either calculated by q-3-D code or approximated using available procedures and empirical formulae in the literature.

Governing Equations and Numerical Technique:

The numerical analysis has been performed with CFD code. This is a finite volume three dimensional Navier Stokes (in fixed frame of reference form for stator or in rotating frame of reference form for rotor) solver. The closure is implemented through the standard $k-\varepsilon$ turbulence model with standard wall functions. The basic equations and relations which are used in this simulation are illustrated as flows:

Continuity Equation:

$$\frac{\partial U_i}{\partial x_i} = 0.0 \tag{1}$$

Momentum Equation in Fixed Frame of Reference:

$$\frac{\partial U_i}{\partial t} + U_j \frac{\partial U_i}{\partial x_j} + \frac{1}{\rho}\frac{\partial P}{\partial x_j} - \frac{\partial}{\partial x_j}\left[(\nu + \nu_t)\left(\frac{\partial U_i}{\partial x_j} + \frac{\partial U_j}{\partial x_i}\right)\right] = 0 \tag{2}$$

In rotating frame of reference Eq.2 can be expressed as follows

$$\frac{\partial U_i}{\partial t} + U_j \frac{\partial U_i}{\partial x_j} + \frac{1}{\rho}\frac{\partial P}{\partial x_i} - \frac{\partial}{\partial x_j}\left[(\nu + \nu_t)\left(\frac{\partial U_i}{\partial x_j} + \frac{\partial U_j}{\partial x_i}\right)\right] = 2\varepsilon_{ijk}\Omega_j U_k + \Omega_i \Omega_j x_j - \Omega_j \Omega_j x_i \quad (3)$$

Turbulence Model Equations: In the derivation of the $k-\varepsilon$ model, it was assumed that the flow is fully turbulent, and the effects of molecular viscosity are negligible (Launder ,1972). The present $k-\varepsilon$ model is therefore valid only for fully turbulent flows. The turbulence kinetic energy, k, and its rate of dissipation, ε are obtained from the following transport equations:

$$\frac{\partial}{\partial t}(\rho K) + \frac{\partial}{\partial x_i}(\rho K u_i) = \frac{\partial}{\partial x_j}\left[\left(\mu + \frac{\mu_t}{\sigma_k}\right)\frac{\partial K}{\partial x_j}\right] + G_k + G_b - \rho\varepsilon - Y_M + S_k \quad (4)$$

$$\frac{\partial}{\partial t}(\rho\varepsilon) + \frac{\partial}{\partial x_i}(\rho\varepsilon u_i) = \frac{\partial}{\partial x_j}\left[\left(\mu + \frac{\mu_t}{\sigma_\varepsilon}\right)\frac{\partial \varepsilon}{\partial x_j}\right] + C_{1\varepsilon}\frac{\varepsilon}{K}(G_k + C_{3\varepsilon}G_b) - C_{2\varepsilon}\rho\frac{\varepsilon^2}{K} + S_\varepsilon \quad (5)$$

The turbulent (or eddy) viscosity, μ_t is computed by combining k and ε as follows:

$$\mu_t = \rho C_\mu \frac{K^2}{\varepsilon} \quad (6)$$

The model constants $C_{1\varepsilon}, C_{2\varepsilon}, C_\mu, \sigma_k$ and σ_ε have the following default values

$C_{1\varepsilon} = 1.44$ $C_{2\varepsilon} = 1.92$ $C_\mu = 0.09$ $\sigma_\varepsilon = 1.3$ $\sigma_k = 1.0$

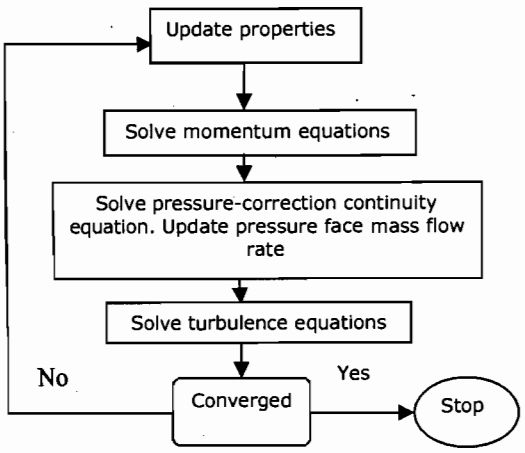

Fig.1: Segregated Algorithm Process

Above equations are solved using implicit segregated solver algorithm. As shown in Fig.1, this algorithm is based on solving the govern equations sequentially (i.e segregated from one another). Momentum, turbulence kinetic energy and turbulence dissipation rate equations were discretized by second order Upwind scheme. In order to satisfy the mass and momentum conservation laws, pressure and velocity were coupled by SIMPLE (Pantankar, 1972and1980) method. in order to check the convergence of the present code, the velocity components, turbulence kinetic energy, turbulence dissipation and continuity residual values were calculated. The solution is said to be converging when each value of the previous residual is less than 10^{-5}.

Boundary Conditions: A periodic boundary condition is used for all flow quantities at blade to blade interface. For purpose of generating high quality mesh, the computational domain was divided into two zones, one zone is inlet and rotor regions and the other is the stator and outlet regions. The boundary plane between the two regions (especially between rotor and stator) is treated as so-called mixing plane (Ruprecht *et al.*, 1999). The atmospheric pressure and constant turbulence kinetic and dissipation energies are prescribed at the inlet. The velocity components are calculated at outlet to consider different flow conditions.

Axial Flow Fan Geometry: The present fan was designed by using modified q-3-d method. This method based on solving the meridional through flow using streamline curvature numerical approach to determine averaged stream surfaces. These stream surfaces are transformed conformally into two dimensional planes to select the blade elements using 2D experimental cascade data. For more information and details about this method (Inoue *et al.*, 1984 and Li Zhe *et al.*, 1996). The basic characteristics of the blades are as follows:-

Outer diameter at inlet	654 mm
Outer diameter at rotor and stator regions	540 mm
Hub/tip ratio	0.630
Design flow rate coefficient	0.294
Design pressure coefficient	0.240
Vortex design	free vortex
Rotor blade number	9
Rotor stagger angle	53 .9 ° / 70 ° from hub to tip
Rotor chord	88 mm/57mm from hub to tip
Stator blade number	15
Stator chord	100 mm
Rotational speed	2900 rpm
Blade profile	NACA65

Grid Generation: As shown in Fig.2, the computational mesh used in the present simulation consists of two types of mesh which are (a) quadrilaterals which are used to mesh the rotor blade, stator blade and the region surrounding the rotor blade.

(b) triangles which are used to mesh the reset of domain. Also as shown in Fig.2, the mesh is condensed at rotor and stator leading and trailing edges so as to capture the most of the important flow field properties at these regions. As indicated by L. Sbard- ella (2001) and verified by the present work, this type of grid has high quality and high ability to predict most of the viscous flow phenomena. The total number of grid points for whole domain is 67052 nodes.

Results and Discussion

In order to study the behavior of flow behind the rotor blades and stator regions, a detailed analysis of static pressure coefficient, velocity components, turbulence intensity and vorticity were made at constant axial-coordinate surface located at 17.28 mm out of the trailing edge of the rotor row and at stator region.

Determination of Vortex and Wake Behind the Rotor Row: Contour plots as shown in Fig.3 and Fig.4 for static pressure coefficient and axial velocity Respectively were used to identify the region of wake and vortex which indicated properly by either a reduction in axial velocity or reduction in static pressure coefficient. Fig.3 indicates an existence of negative static pressure in case of large flow rate, hence this case is physically rejected. In case of small flow rate the static pressure increase from hub to tip and insures that an existence of stronger vortex near the hub than the design case. This is clearly appeared in Fig.4(c) which shows a decrease in axial velocity near the hub and at the lower right corner. Fig.4(a) indicates that the axial velocity in the center of the plane is nearly constant and it is small in the wake and near wall regions(due to viscous effect). Also it is seen from Fig.4 the variation of axial velocity in case of design value is smaller than the other two cases. Note that for all constant axial coordinate plane presented in this work, the direction of rotation is from right to left.

Range of Vortex at Rotor Exit: Range of vortex can be determined from the radial velocity contour plots or axial flow velocity plot at radial position. This range is indicated by a positive increase in radial velocity. These contours are shown in Fig.5. As shown in that figure the minimum range of the positive radial velocity was predicted at design flow rate.

As stated previously the wake and vortex can be predicted by the sudden decrease in axial velocity hence its range can be predicted from x-y plot of axial velocity at radial position. Fig.6(a) shows the region of sudden decrease in axial velocity at rotor exit near the hub at different flow rate. It is seen from that figure maximum region of reduction of axial velocity occurs at lower flow rate. This means that the range of wake at lower flow rate is wider than that at high flow rate.

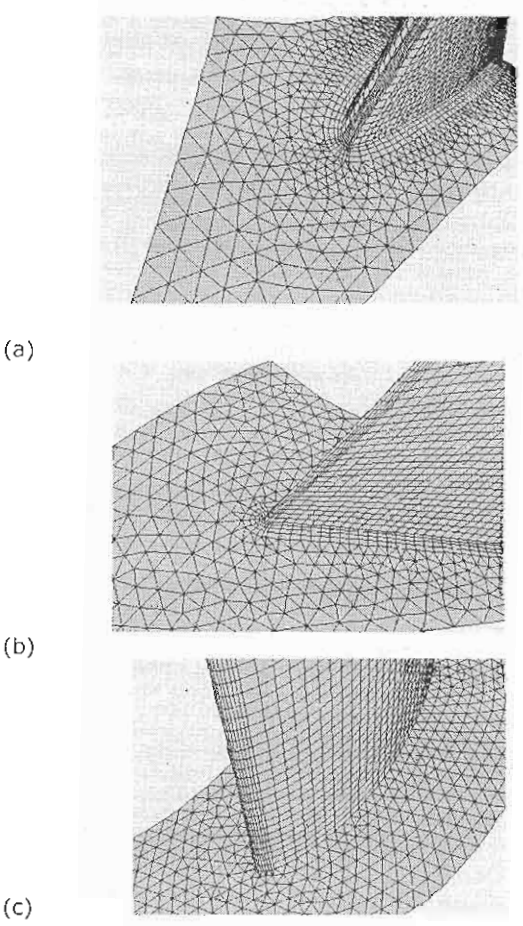

Fig.2: Sample of Grid Generation (a). Near Rotor Leading Edge (b). Near Rotor Trailing Edge (c). at Stator. For All Figures the Lower Surface is Hub

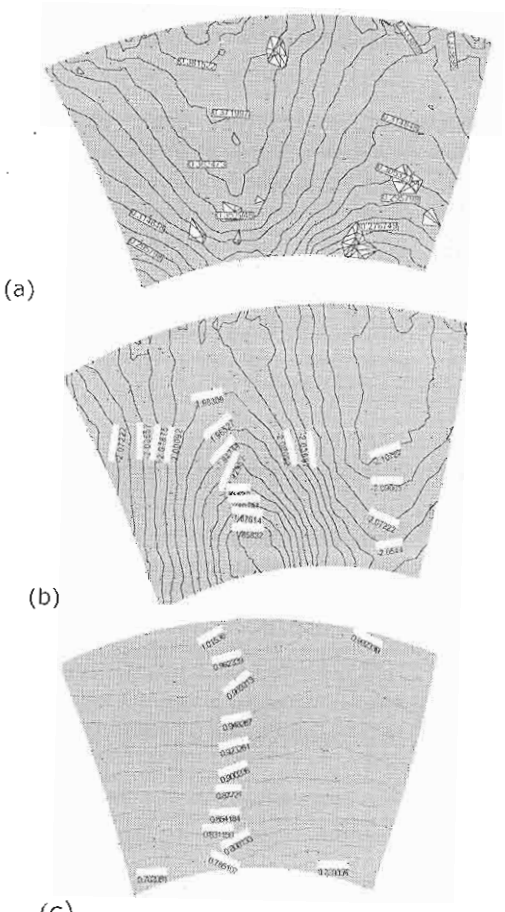

Fig.3: Contour of Static Pressure Coefficient at Axial Location 470mm (17.28 mm from exit of rotor) (a)at $\phi = 0.294$(b) at $\phi = 0.427$(c)at $\phi = 0.244$

Validation of the Present Work: For the purpose of validation of the present work, the velocity components which are shown in Fig.6 were compare with the experimental results which found in (Motoo, *et al.*, 1982; Chang Soo (2000) and Chen(1999), Esevadeordal (2000)) . It was found that the two results have similar physical behavior.

Strength of Wake and Vortex Flows at Rotor Exit: The strength of wake and vortex flow was determined by studying the turbulence intensity contour and vorticity at the exit of rotor. In fact minimum turbulence intensity indicates weak wake and vortex flow. As clearly observed from Fig.7 increasing flow rate results in high turbulence intensity hence a strong existence of wake and vortex flows.

Vorticity is a measure of the rotation of a fluid element as it moves in the flow field and it is defined as the curl of the velocity vector ($\xi = \nabla \times \vec{V}$). As shown in Fig.8, increase in flow rate causes an increase in vorticity.

Also Fig.8 indicates that, for all flow rate the vorticity near the case and hub is larger than the vorticity at mid span, mainly due to viscous effect at that regions. It is seen from Fig.8 that, vorticity near the case is higher than that near the hub due to effect of relative motion between the case (fixed part) and the adjacent rotating fluid.

Study of Stator Flow Pattern: Fig.9 shows the variation of static pressure at stator hub at different flow rates. It is seen from that figure the stator becomes inefficient in case of large flow rate because of existence of negative static pressure in both sides (suction and pressure) of the stator. Also it is seen from that figure maximum static pressure occurs when the flow rate is small.

Fig.10 shows the velocity vector at stator hub. It is easily observed that a vortex flow at stator pressure side in case of high flow rate and vortex flow at stator suction side in case of low flow rate while the flow in case of design flow rate is smooth. The appearance of

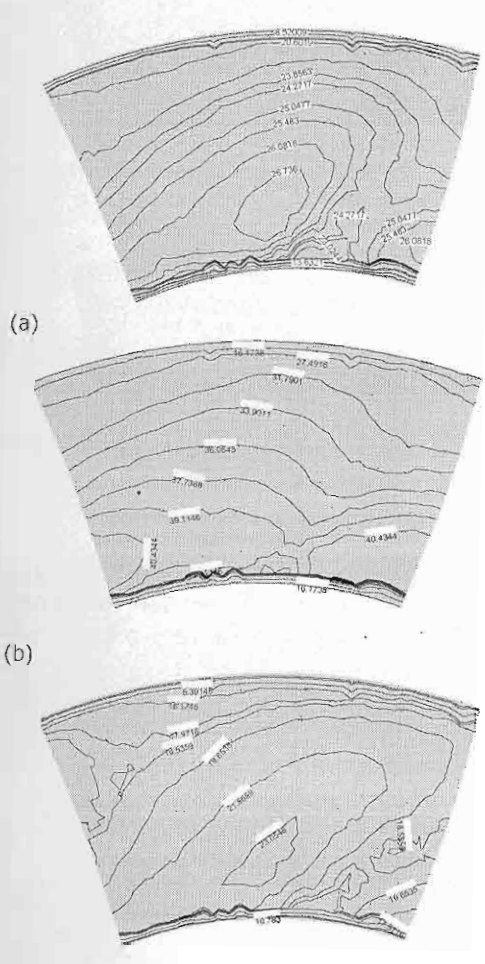

Fig.4: Contour of Axial Velocity at Axial Location 470mm (17.28mm from exit of rotor)
(a) at $\phi = 0.294$ (b) at $\phi = 0.427$ (c) $\phi = 0.244$

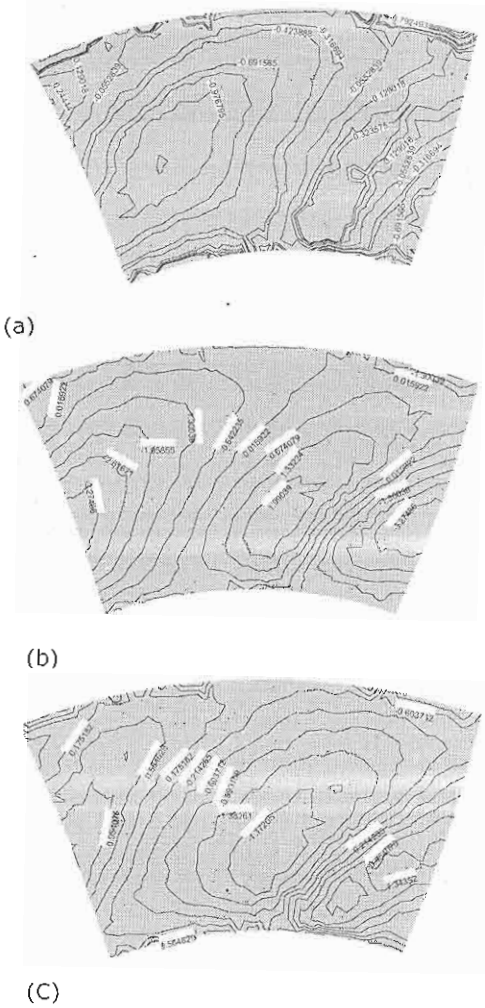

Fig.5: Contour of Radial Velocity at Axial Location 470mm (17.28 mm from exit of rotor)
(a) at $\phi = 0.294$ (b) at $\phi = 0.427$ (c) $\phi = 0.244$

strong vortex flow at pressure side is due to premature flow separation caused by the adverse pressure and non-negligible influence of the hub. It results in the production of thick boundary flow on the pressure surface which causes the vortex flow.

Fig.11 (a) and (b) correspond the velocity distribution on stator suction side at lower flow rate and on stator pressure side at large flow rate. Fig.11 (a) shows

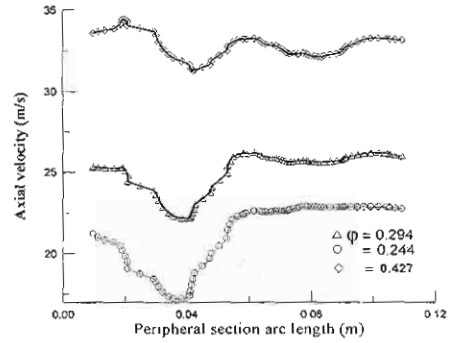

(a)

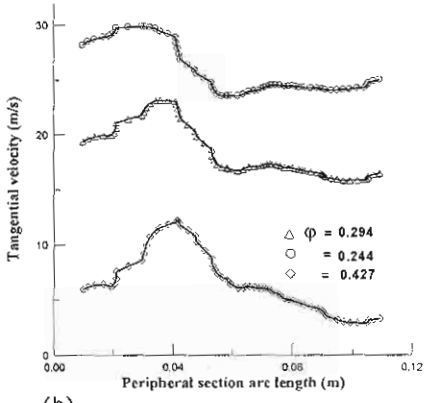

(b)

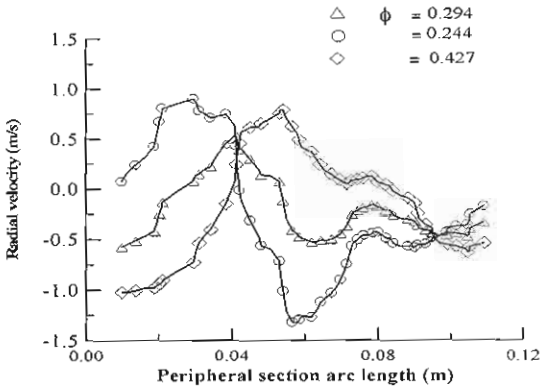

(C)

Fig.6: Flow Velocity at Rotor Exit (near hub) at Different Flow Rate (a) Axial Velocity (b) Tangential Velocity (c) Radial Velocity

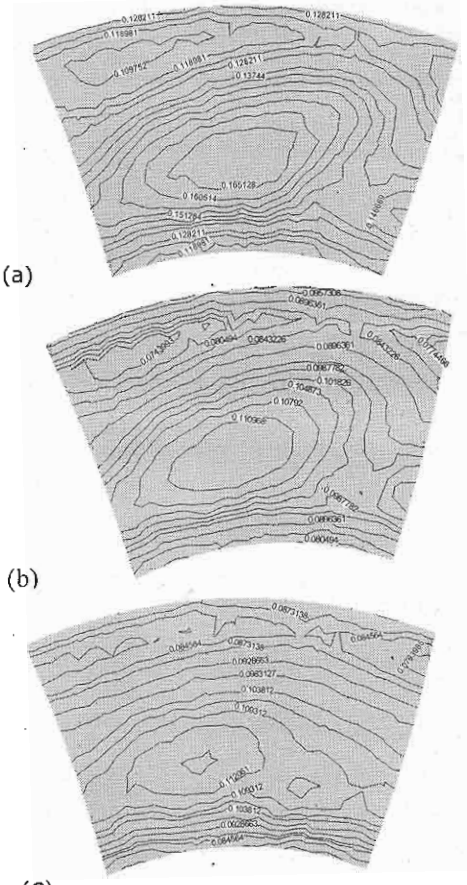

(a)

(b)

(c)

Fig.7: Contour of Turbulent Intensity at Axial Location470mm (17.28 mm from exit of rotor) (a) at $\phi = 0.294$ (b) at $\phi = 0.427$ (c) at $\phi = 0.244$

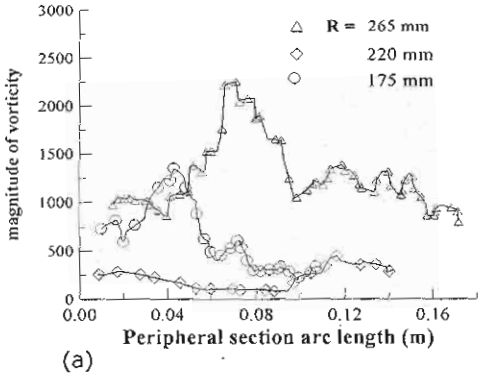

(a)

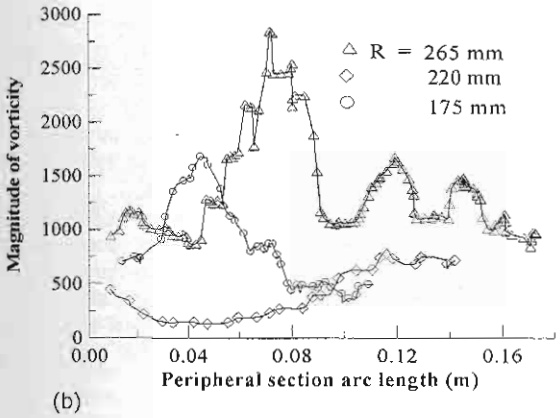

(b)

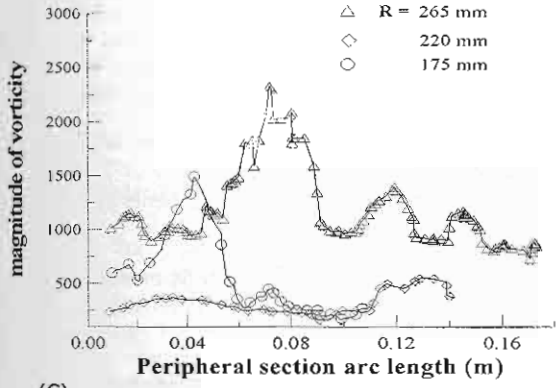

(C)

Fig.8: Magnitude of Vorticity at Different Rotor Exit Radial Position and Costant Axial Location(470 mm)

(a) at $\phi = 0.294$ (b) at $\phi = 0.427$ (c) at $\phi = 0244$

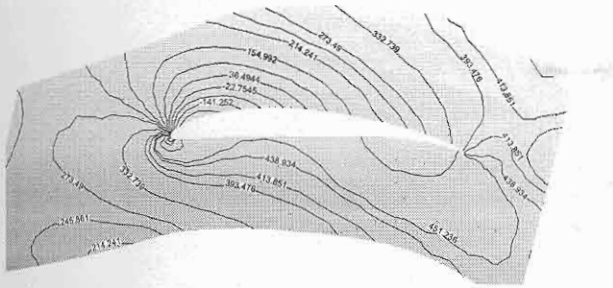

(a)

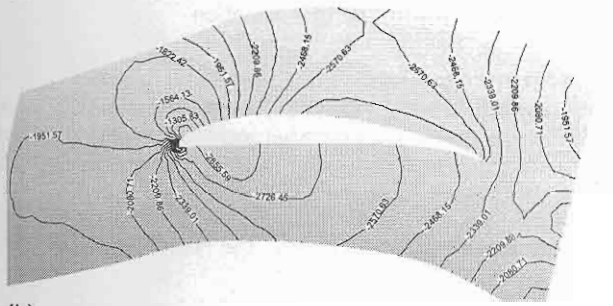

(b)

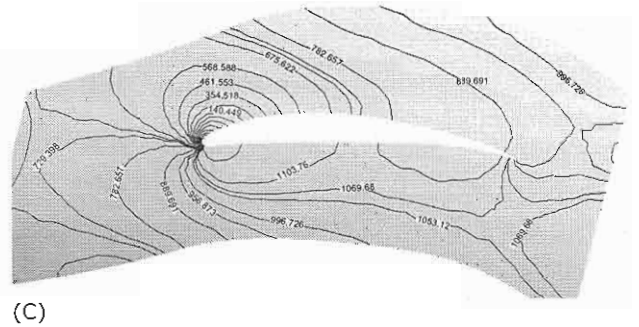

(C)

Fig.9: Static Pressure (Pa) at Stator Hub Region

(a) at $\phi = 0.294$ (b) at $\phi = 0.427$ (c) at $\phi = 0244$

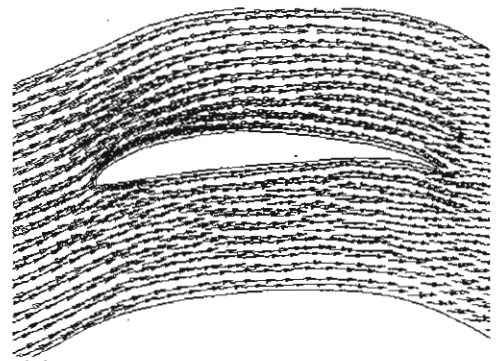

(a)

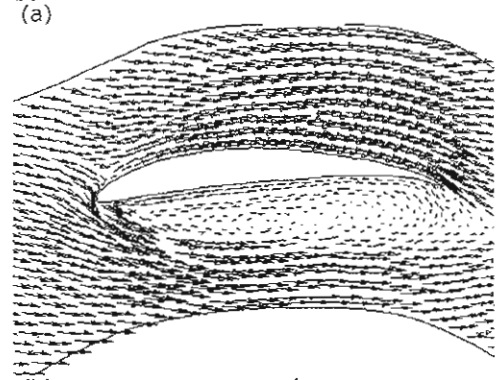

(b)

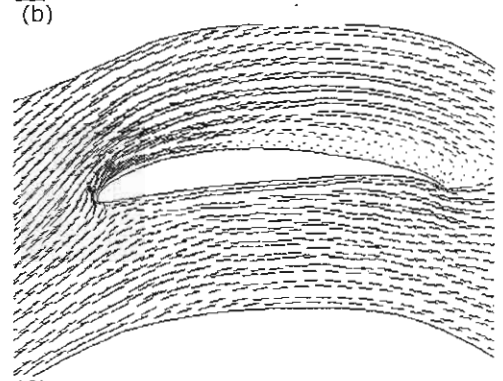

(C)

Fig.10: Velocity Vector at Stator Hub Region

(a) at $\phi = 0.294$ (b) at $\phi = 0.427$ (c) at $\phi = 0.244$

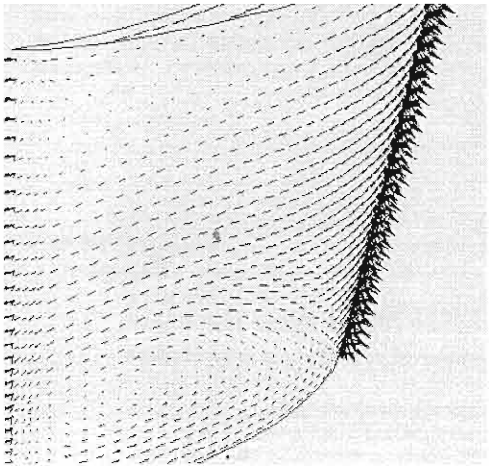

(a)

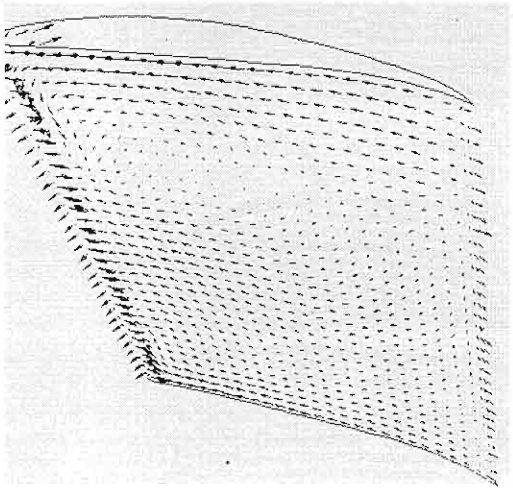

(b)

Fig.11: Velocity Vector at (a) Stator Suction Side at Small Flow Rate (b) Stator Pressure Side at Large Flow Rate

existence of vortex flow at stator suction side near the hub and the flow try to move from pressure side to suction side at stator leading edge. Kind of this flow at leading edge indicates existence of leading edge vortex.
It is observed clearly from Fig. 11(b) that, a vortext flow occurs at stator pressure side in case of large flow rate and center of core of this vortext is far away from hub.

Conclusion

The three dimensional flow field in axial flow fan which consists of rotor and stator has been studied by means of CFD code based on solving Navier stoke equations, with standard $k-\varepsilon$ turbulence model for closure. Detailed analysis of the 3D flow field has been conducted for different flow conditions. The results are summarized as follows:

- The computations provided detailed information on structure of vortex and wake at rotor exit and stator region.
- The variation of flow rate influences the flow at stator region significantly. Lower flow rate causes a vortex flow at stator suction side while a large low rate causes a vortex flow at stator pressure side.
- The flow rate has influence on the flow at rotor exit. As flow rate is decreased the range of the wake and vortex becomes wider at rotor exit.

Nomenclature:

U_i	mean velocity component
R	Radius
t	time
P	pressure
x_j	Cartesian coordinate
G_k	Generation of turbulence kinetic energy due to mean velocity gradient
G_b	generation of turbulence kinetic energy due to buoyancy
K	turbulence kinetic energy
Y_M	Contribution of fluctuating distribution in compressible turbulence over all dissipation rate (neglected)
S_k	turbulence kinetic energy source term
S_ε	turbulence dissipation rate source term
ν	kinematic viscosity
ν_t	turbulence kinematic viscosity
ε_{ijk}	cross product tensor
Ω_j	rotation vector
ρ	density
μ	viscosity
μ_t	turbulence viscosity
ε	turbulence rate of dissipation

References

Alessandro Corsini, Computational investigation of flow phenomena in an isolated axial fan rotor using Navier-stokes rocedure R and D(TeT) coorperation project I-28/98

Launder, B. E. and D.B. Spalding;1972. Lectures in mathmetical models of the tuebulence, Academic Press, London, England

Chang soo Kim; 2000. Flow characteristics of Axial flow fan, The sixth Asian international conference on fluid machinery 18-21 ; 139-144

Chen N.X., Xu Y. J. and W. G. Huang; 1999. Numerical study on the three dimensional turbulent flow in low speed axial single rotor compressor and its comparison with experiment, Fourth International symposium on experimental and computational Aerothermodynamics of internal flows, 151-160

Chen Naixing; Z.Wang; S.Wang and G.Feng; 2001.A Study on Secondary Flow Pateren and Blad Bowing Effects in Turbine Bladings 5th International Symposium on Experimental and Computational Aerothermodynamics of Internal Flows, Gdansk, Poland, 19-43

Estevadeordal, J., S.Gogineni, *et al*., 2000. Flow field in a low-speed axial fan: a DPIV investigation, Experimental thermal and fluid sci., 23, 11-21, ELSEVIER

János Vad and Ferenc Bencze;1998. Three-dimensional flow in axial flow fans of non-free vortex design, International J. of Heat and Fluid Flow, vol. 19,601-607

Li Zhe and Wu Keqi; 1996. Quasi three dimensional flow design and characteristics of diagonal flow impeller With circular arc plate, 675-678

Sbardella, L. and M. Imregun; 2001. Linearized Unsteady Viscous Turbomachinery Flows Using Hybrids Grids, Transactions of The ASME, J. of Turbomachinery Vol.123,568-582.

Masaniro Inoue; 1997. Vortex and Turbomachinery , The fifth Asian International Conference on Fluid Machinery, Seoul, Korea, 117-131.

Motoo K., M. Inoue, *et al.*, 1982. "Measurement of three dimensional flow field behind an impeller by means of periodic multi sampling with a slanted hot wire" Bulletin of the JSME, vol 25, No 209, 1674-1681

Inoue M., Wu Keqi, *et al.*, 1984. A design of Diagonal Impeller by Means of SCM and cascade data, Proc. Of China-Japan Joint Conference on hydraulic Machinery and equipment, 21-30

Mou-Jin Zhang, M. J. Pomfret and C.M. Wong;1996. Three dimensional Viscous Flow Simulation In a backswept Centrifugal Impeller at the design point, Computers &fluids Vol. 25, no. 5, 497-507 .

Pantankar S.V. and D.B. Spatding; 1972. "Calculation Procedure for heat transfer, mass and momentum in three dimensional parabolic flows" International J.of Heat and Mass Transfer, V.15,

Pantankar S.V., 1980. Numerical Heat Transfer and Fluid flow, MC Graw-Hill,

Su Moming, Gu Chuan-gang and Miao Yong-miao; 1996.Study of three dimensional Viscous Flow Field In axial flow fan, International Gas and Aeroengine Congress and Exhibition Birmingham, UK- June 10-13,.

Ruprecht, A. and C. Bauer; 1999. Parallel Computation of stator-rotor interaction in axial turbine, ASME PVP conference, CFD Symposium, Boston,

Novak, R. A.," 1967. Streamline curvature computing Procedures for fluid-flow Problems" Transactions of the ASME, J. of Eng. for power, 478-490